

Artificial Neural Network Model Using Immune-infiltration Modules for Endometrial Receptivity Assessment of Implantation Failure

Bohan Li

Capital Medical University Beijing Obstetrics and Gynecology Hospital

Hua Duan (✉ duanhua@ccmu.edu.cn)

Capital Medical University Beijing Obstetrics and Gynecology Hospital <https://orcid.org/0000-0002-5123-5147>

Sha Wang

Capital Medical University Beijing Obstetrics and Gynecology Hospital

Jiajing Wu

Capital Medical University Beijing Obstetrics and Gynecology Hospital

Yazhu Li

Capital Medical University Beijing Obstetrics and Gynecology Hospital

Research

Keywords: Immune infiltration, Endometrial receptivity, Implantation failure, Deep machine learning, Artificial neural network

Posted Date: January 17th, 2022

DOI: <https://doi.org/10.21203/rs.3.rs-860927/v2>

License:  This work is licensed under a Creative Commons Attribution 4.0 International License.

[Read Full License](#)

Artificial neural network model using immune-infiltration modules for endometrial receptivity assessment of implantation failure

1 Bohan Li MD,¹ Hua Duan PhD, MD,^{1*} Sha Wang PhD, MD,¹ Jiajing Wu MD,² Yazhu Li MD,
2 ¹

3 ¹Department of Minimally Invasive Gynecologic Center, Beijing Obstetrics and Gynecology
4 Hospital, Capital Medical University, Beijing 100006, China.

5 ²Capital Medical University School of Basic Medical Sciences, Beijing 100069, China.

6 * **Correspondence:**

7 Hua Duan

8 duanhua@ccmu.edu.cn

9 **Abstract**

10 **Objectives:** This study was anchored on the state of local immune-infiltration in the endometrium,
11 which acts as critical factors affecting embryonic implantation, and aimed at establishing novel
12 approaches to assess endometrial receptivity for patients with IVF failure.

13 **Methods:** Immune-infiltration levels in the GSE58144 dataset (n=115) from GEO were analyzed by
14 digital deconvolution and validated by immunofluorescence (n=30), illustrating that dysregulation of
15 the ratio of M ϕ 1 to M ϕ 2 is an important factor contributing to implantation failure. Then, modules
16 most associated with M1/M2 macrophages (M ϕ s) and their hub genes were then selected by weighted
17 gene co-expression network and univariate analyses, then validated by GSE5099 macrophage dataset,
18 qPCR analysis (n=16), and western blot. It revealed that closely related gene modules dominated

19 three biological processes in macrophages: antigen presentation, interleukin-1-mediated signalling
20 pathway, and phagosome acidification, respectively. Their hub genes were significantly altered in
21 patients and related with ribosomal, lysosome, and proteasomal pathways. Finally, the artificial
22 neural network (ANN) and nomogram models were established from hub genes, of which efficacy
23 was compared and validated in the GSE165004 dataset (n=72). Models established by the selected
24 hub genes exhibited excellent predictive values in both datasets, and ANN performed best with an
25 accuracy of 98.3% and an AUC of 0.975 (95% CI 0.945-1).

26 **Conclusions:** Macrophages, proven to be essential for endometrial receptivity, were regulated by
27 gene modules dominating antigen presentation, interleukin-1-mediated signalling pathway, and
28 phagosome acidification. Selected hub genes can effectively assess endometrial dysfunction
29 receptivity for IVF outcomes by the ANN approach.

30 **Keywords:** Immune infiltration, Endometrial receptivity, Implantation failure, Deep machine
31 learning, Artificial neural network

32

33 **1. Introduction**

34 Recurrent implantation failure (RIF) is one of the most frustrating and difficult areas in reproductive
35 medicine because the etiology is often unknown and there are few evidence-based diagnostic and
36 treatment strategies. Defective endometrial receptivity is currently becoming a critical theory in the
37 study of this disease. Endometrial receptivity, is a complex process that enables embryonic
38 attachment, invasion, and development. For healthy females, during the secretory phase, the window
39 of implantation (WOI) lasts from 3 to 6 days. In certain inflammatory or anatomical cases, this
40 window can be narrowed or displaced to inhibit normal implantation, resulting in infertility or loss of

41 pregnancy (1). Therefore, a receptive endometrium is a prerequisite for successful embryonic
42 implantation. Defective endometrial receptivity is often associated with RIF and unexplained
43 infertility (UI). However, a lack of understanding of defective endometrial receptivity has led to poor
44 diagnosis and treatment. The current diagnostic tests for endometrial receptivity anomalies include
45 sonography (endometrial thickness, blood flow, and morphology), histopathology (integrin $\alpha\beta3$,
46 leukemia inhibitory factor, vascular endothelial growth factor, and uterine natural killer cells), as well
47 as electron microscopy of endometrial cell morphology. However, these methods have a limited
48 clinical guidance (2). An emerging assay, Endometrial Receptivity Array (ERA), guides clinical
49 practice by assessing endometrial receptivity status through microarray analysis of 238 genes (3).
50 However, the clinical significance of the test has not been fully established (4). The high number of
51 genes that are required for analysis and strict requirements for sample storage conditions lead to high
52 costs and difficulties in clinical practice.

53 Immune status of the endometrium is closely associated with normal reproductive functions(5).
54 Trophoblast cells of the implanted blastocyst invade the endometrium of the maternal uterus by
55 forming the placenta. Endometrial mesenchymal cells undergo a decidual response (called
56 decidualization) and establish an environment that is conducive for trophoblast invasion. Trophoblast
57 implantation and placenta formation require appropriate maternal immune tolerance to the hemi
58 allogeneic foetus. After embryonic implantation and decidual development, the number of leukocytes
59 in the uterus change significantly (6). Natural killer (NK) cells and macrophages predominate during
60 the early gestation period. Macrophages, which account for approximately 20-30% of total
61 infiltrating leukocytes, play an essential role in fetal tolerance, trophoblast invasion, and tissue as
62 well as vascular remodelling (7). The immune environment of the endometrium is in a dynamic
63 balance due to hormonal regulation and stress responses to clinical operation and dysbacteriosis.
64 Therefore, endometrial receptivity assessment based on immune-related modules can predict

65 implantation outcomes and predict pregnancy timing after a uterine cavity procedure (induced
66 abortion, adhesiolysis, and polypectomy) or other therapies (antibiotics, hormones etc). However,
67 few studies have evaluated its value in assessing endometrial receptivity.

68 Due to genetic heterogeneity, epistatic interactions, and environmental factors, identification of a
69 single gene or pathway underlying the complex traits is difficult (8). Integration of gene expression is
70 a key method for solving this problem. Network methods have been used to identify and characterize
71 various biological interactions and have helped in predicting gene functions (9). In this study, we
72 used weighted gene co-expression network analysis (WGCNA) to establish gene modules and
73 evaluated their association with integrated clinical traits(10). The predictors selected in this approach
74 have representative biological structures and functions. Previous evaluation models were established
75 by regression equations. However, measurement errors across platforms and patients'
76 individualization often make it difficult to guarantee the consistency of results, which in turn affects
77 repeatability of the method. The artificial intelligence approach can be used to guarantee the
78 consistency of results across platforms and populations by training the programs with specific
79 patterns. The artificial neural network (ANN) is an artificial intelligence (machine learning) method
80 that works similarly to the human brain(11). Its incorporated feature variables, also known as
81 predictors, input variables and covariates, are the input signals that inform pattern recognition. Each
82 characteristic variable is weighted according to its clinical significance. The task is accomplished by
83 dendrites in the biological nervous system. An activation function sums the weighted signals (12).
84 We performed WGCNA to identify immunological factors that were most associated with defective
85 endometrial receptivity and used them to develop a fertility prognostic model through ANN. The
86 results were validated in different platforms and populations to obtain a more practical and reliable
87 approach for endometrial receptivity assessment.

88 **2. Methods**

89 **2.1 Datasets and patient selection**

90 All datasets were selected from chip microarrays. The GSE58144 dataset, containing 43 RIF patients
91 and 72 controls, was used for immune infiltration analysis, hub gene selection, and machine deep
92 learning prognostic model establishment. The GSE5099 dataset is a three replicate measure dataset of
93 gene expression matrices of M ϕ 1 and M ϕ 2 that was used to validate the association between hub
94 genes and macrophage polarization. The GSE165004 dataset includes 48 implantation failure (IF)
95 patients and 24 controls, and was used to validate hub gene expression differences and machine deep
96 learning prognostic model. Details of the microarrays are available in supplementary Table 1.

97 Validation of M ϕ 1/M ϕ 2, mRNA and protein levels were performed using clinical samples. Ethical
98 approval for this study was obtained from the Research Ethics Committee of the Beijing Obstetrics
99 and Gynecology Hospital. Experiments were performed (under protocol number 2017-KY-082-02)
100 based on the Helsinki Declaration of 1975 (revised in 2013). Patients eligible for hysteroscopy were
101 required to sign an informed consent before surgery. Samples from endometrial biopsies were
102 acquired at Beijing Obstetrics and Gynecology Hospital. The inclusion criteria for patients were: i.
103 Those aged less than 40 years; ii. Those whose sex hormone levels, including follicle-stimulating
104 hormone, luteinizing hormone, testosterone, estradiol and prolactin, were within normal ranges and
105 iii. Those without endometriosis, fibroids, active or a history of pelvic inflammatory disease or other
106 medical comorbidities (hyperprolactinemia, thyroid disease etc). Study participants in the control
107 group (n=14) had at least one live birth while others (n=16) were examined for unexplained infertility
108 or implantation failure. Basic demographic characteristics for each group are presented in
109 supplementary Table 2. Specific flow of the study design is shown in Fig. 1.

110 **2.2 Processing of primary datasets**

111 Pre-processing and normalization of microarray datasets based on raw data of the Affymetrix
112 platform (GSE5099) were performed using the affy package (in R, version 3.6.2) (13) with the
113 following methods: i. Robust multi-array average (RMA, for background correction) (14); ii.
114 Quantile (for normalization) (15); iii. pmonly (perfect match correction) (16) and iv. Median polish
115 (as a summary method) (17). For the microarray datasets that were based on the Agilent platform
116 (GSE58144 and GSE165004), Biobase and limma packages (in R, version 3.6.2) were used for pre-
117 processing and normalization after the data had been converted to log (base 2). The RMA and
118 normalizeBetweenArrays methods were used for background correction and normalization,
119 respectively(18). Annotation files for different microarray platforms were downloaded from the
120 NCBI GEO database (19).

121 **2.3 Digital deconvolution of bulk tissues**

122 Cell-type deconvolution was performed using CIBERSORTx (<http://cibersortx.stanford.edu>), which
123 is an analytical tool developed by Newman et al. (20) to impute gene expression profiles and provide
124 estimations of the abundances of immune cell infiltration levels in mixed cell populations, using gene
125 expression data. We used the LM22 gene signature matrix for 22 immune cell types. CIBERSORTx
126 was run with batch correction and 100 permutations. Barplot and vioplot were established using the
127 plot function (in R, version 3.6.2).

128 **2.4 Immunofluorescence**

129 From each sample, 5 μm sections were prepared and dewaxed in xylene, dehydrated using graded
130 alcohol and rinsed in distilled water. For antigen retrieval, sections were boiled in citric saline (10
131 mmol/L, pH 6.0) for half an h. Then, samples were treated with 3% hydrogen peroxide solution for
132 25 min to block the activity of endogenous peroxidase, blocked using 3% bovine serum albumin
133 (BSA, Servicebio, Wuhan, China) for 30 min at room temperature, after which they were incubated

134 at 37°C for 1 h with primary antibodies, which included mouse anti-CD68 (ab201973, Abcam,
135 dilution 1:200), rabbit anti-CD86 (13395-1-AP, Proteintech, dilution 1:200) for M ϕ 1 as well as
136 mouse anti-CD68, rabbit anti-CD86 (13395-1-AP, Proteintech, dilution 1:200) for M ϕ 2. Next,
137 sections were rinsed 3 times in phosphate-buffered saline (PBS) and stained using anti-rabbit-Alexa
138 Fluor® 488 (ab150073, abcam) and anti-mouse-Alexa Fluor® 594 (ab150064, abcam) for 1 h at
139 room temperature (both Invitrogen). Slides were mounted in the SlowfadeGold reagent containing
140 DAPI (Thermofisher, Landsmeer, The Netherlands) and examined using a NIKON CORPORA
141 microscope (Nikon, Japan). The percentage of M ϕ 1 or M ϕ 2 was obtained by counting fluorescence
142 positive cells and dividing them by DAPI signal points using Image J (Version 1.50b), respectively.

143 **2.5 Weighted gene co-expression network**

144 The network module was established using the WGCNA package (in the R environment, version
145 3.6.2) in GSE58144 dataset (21). To minimize noise in the gene expression dataset, data was filtered
146 as follows. Pearson correlation analysis was used to rank all genes according to their association with
147 M ϕ 1/M ϕ 2. Correlations between genes and M ϕ 1/M ϕ 2 were established at a cut-off of $p \leq 0.05$. To
148 reduce the computational burden and enhance signals in our data, we used 2,185 of the 5,531 genes
149 with the greatest variability ranked by the variance in our initial network construction with a cut-off
150 value of $\text{var} > 0.05$ (21). By definition, module genes are highly connected (i.e., module genes tend
151 to have relatively high connectivity). Therefore, for module detection, restricting analysis to the most
152 connected genes should not lead to a major loss of information. Then, we performed cluster analysis
153 of 2,185 genes in these 115 patients. The theory of network construction algorithm has been
154 previously described (22). Briefly, for co-expression module identification, Pearson correlation
155 matrices were first generated (average linkage method) for all pairwise genes. An adjacency matrix
156 was then constructed using a "soft" power adjacency function, $a_{ij} = |\text{cor}(x_i, y_j)|^\beta$. Based on scale-

157 free topology criteria ($R^2=0.85$), we selected a power of $\beta=10$. In WGCNA, a soft threshold
158 parameter, beta, of the power function was used to ensure that the co-expression network (adjacency
159 matrix) best approximates scale-free topology. This adjacency matrix was then transformed into a
160 topological overlap matrix to measure relative gene interconnectedness and proximity. Finally, gene
161 co-expression modules corresponded to branches of the resulting hierarchical clustering tree
162 (dendrogram). To ensure that genes in the analyzed network exhibited sufficient correlation, we set
163 the weight threshold of the co-expression network to 0.03. Uniform Manifold Approximation and
164 Projection (UMAP) analysis and visualization of the modules was performed using the umap
165 package (in R, version 3.6.2). Visual network diagram was constructed using Cytoscape (version
166 3.4.0).

167 **2.6 Enrichment analysis of functional categories**

168 The STRING v11.5 online tool (<https://string-db.org/>) was used for functional enrichment analysis of
169 the gene module that was most associated with endometriosis, identified after WGCNA analysis. In
170 the enrichment analysis, Gene Ontology (GO) terms (including Biological Process BP, Cellular
171 Component CC, and Molecular Function MF) as well as the Kyoto Encyclopedia of Genes and
172 Genome (KEGG) were used to evaluate functional categories and pathways for genes involved in the
173 module. Correlations with M ϕ 1/M ϕ 2 for all genes was calculated using the cor function in R
174 environment, version 3.6.2. Then, the GOplot package (in the R environment, version 3.6.2) was
175 used to visualize GO enrichment analysis results and their regulatory conditions. The formula for
176 calculating Z-score is $z - score = \frac{(up-down)}{\sqrt{count}}$, which is a value that indicates whether GO terms are
177 more likely to be decreased (negative value) or increased (positive value). Gene-set enrichment
178 analysis (GSEA) was performed on the GSE5099 dataset using the “ClusterProfiler” (24) package in
179 R. The Broad Molecular Signature Database (MSigDB v7.0) dataset in the Kyoto Encyclopedia of

180 Genes and Genomes (KEGG) (c2.cp.kegg.v7.0.symbols) was used. This database summarizes and
181 presents specifically well-defined biological states and pathway processes. For statistical significance
182 estimation, the GSEA program was run with 1,000 permutations, and correlations between selected
183 genes and other genes were used to rank all genes.

184 **2.7 Quantitative Real-Time PCR Analysis (qRT-PCR)**

185 Total RNA was extracted from each sample with RNAiso Plus (Takara Bio Inc., Shiga, Japan) and
186 quantified with a NanoDrop™ One Spectrophotometer (Thermo Fisher Scientific Inc.,
187 Massachusetts, USA). The First-Strand cDNA Synthesis SuperMix Kit (AT301-3, EasyScript, China)
188 was used to synthesize cDNA from 1 µg of total RNA per sample. The primers used in this study
189 were designed by Sangon Biotech Co., Ltd. Shanghai, China. The sequences are presented in
190 supplementary Table 3. PCRs were performed on an LightCycler 480 PCR System (Roche,
191 Germany) with the protocol for the SYBR Premix Ex Taq™ II (RR820A, Takara). The reaction
192 began at 95°C for 30 seconds for initial denaturation, followed by 35 cycles of 5 seconds at 95°C and
193 34 seconds at 60°C(23). The measurements were repeated three times, and the relative quantification
194 was performed by the comparative CT ($2^{-\Delta\Delta CT}$) method.

195 **2.8 prognostic model establishment and statistics**

196 The ANN prognostic model was implemented using the nnet package in R environment, version
197 3.6.2 (12). To determine the number of units in the hidden layer, the GSE58144 dataset was used:

198 $Average\ Accuracy = \sum_{i=1}^l \frac{TP_i + TN_i}{TP_i + FN_i + FP_i + TN_i} / l$. Moreover, to ensure maximum optimization of the

199 prognostic model, NNET was run with 100 permutations in the GSE165004 dataset for verification.

200 For prognostic model efficacy testing, Z tests were used to determine the significance of the area
201 under the receiver operating characteristic (ROC) curve (AUC) using the pROC package in R,

202 version 3.6.2. Sensitivity, specificity, Youden index (YI), positive predictive value (PPV), and
203 negative predictive value (NPV) were used to assess prognostic values of hub genes and the machine
204 learning model.

205 Comparisons of cell proportions and single gene expression levels between the two groups were
206 performed by Wilcox test. Normally distributed continuous variables were analysed by the Students
207 t-test and paired t-test was used for paired analysis (in R, version 3.6.2).

208 **3. Results**

209 **3.1 Immune infiltration levels on endometrial receptivity**

210 Immune infiltration levels of 22 immune cells in endometrial mixed tissue samples from the
211 GSE58144 dataset were determined using the CIBERSORTx platform. These findings are shown in
212 Fig. 2A. In different groups, there were no significant differences in the percentage of immune cells,
213 except for eosinophils, which were present in deficient levels in the tissues (Fig. 2B). Considering
214 that macrophage polarization may be an important factor in endometrial receptivity, we determined
215 the ratio between M ϕ 1 and M ϕ 2 and found significant differences in M ϕ 1/M ϕ 2 between IF and
216 normal groups ($p=0.019$) (Fig. 2C). We further obtained endometrial tissues from 30 patients within
217 the mid-secretion phase for immunofluorescence detection, and found that the balance between M ϕ 1
218 and M ϕ 2 in the IF group was significantly altered compared to the controls ($p=0.043$), as shown in
219 Fig. 2D&E.

220 **3.2 Macrophage polarization-related gene module functions**

221 As shown in Fig. 3A, genes were clustered into different groups, referred to as modules. The
222 GSE58144 gene set had 7 different gene modules with a high topological overlap. To distinguish the

223 modules, we allocated a colour to each module (including brown, black, Green, turquoise, red, blue,
224 and yellow).

225 Then, we evaluated the pathological correlation for each module by examining the overall correlation
226 of module genes with clinical traits of immune infiltration. The measure of gene significance was
227 defined by the absolute value of the correlation between clinical factors and gene expression levels.
228 Average genetic significance of a particular module is considered module significance (MS). As
229 shown in Fig 3B, three modules (blue, turquoise, and green) exhibited excellent correlations with
230 M ϕ 1/M ϕ 2, that is, -0.42 ($p=3\times 10^{-6}$), -0.35 ($p=10^{-4}$), and 0.32 ($p=5\times 10^{-4}$), respectively. Moreover,
231 there were significant correlations between module membership of the genes within the module and
232 gene significance between these genes and M ϕ 1/M ϕ 2 ($P_{\text{blue}}=1.6\times 10^{-39}$, $p_{\text{turquoise}}=6.6\times 10^{-15}$, and $p_{\text{green}}=0.0093$), as shown in Fig 3C. In Fig. 3D, the integrated molecular profiles of aforementioned
233 three modules are visualized using two-dimensional maps generated by the dimension reduction
234 technique UMAP. In the resulting plot, the samples in the dataset can be grossly divided into two
235 subgroups by the disease, revealing that implantation failure patients have unique profile based on
236 M ϕ 1/M ϕ 2 related modules.
237

238 Then, we performed enrichment analysis of the three modules. We found that the main biological
239 processes of the three modules were the three aspects of macrophage functions (antigen processing
240 and presentation of exogenous peptide antigen via MHC class I, TAP-dependent, $\text{FDR}=4.5\times 10^{-10}$;
241 phagosome acidification, $\text{FDR}=6.2\times 10^{-4}$; interleukin-1-mediated signaling pathway, $\text{FDR}=1.13\times 10^{-13}$), while the corresponding GO-CC and GO-MF terms of the three were also different. KEGG
242 enrichment analysis revealed that the three modules were enriched in ribosomal, lysosome, and
243 proteasomal pathways, respectively (Fig. 4A).
244

245 **3.3 Selection and verification of hub genes associated with M ϕ 1/M ϕ 2**

246 Due to differences in biological roles of the three gene modules and high-levels of consistency in
247 expression among genes within the modules, we selected three hub genes in each of the modules.
248 First, we selected genes that were most associated with modules and M ϕ 1/M ϕ 2 based on the median
249 of the membership in the module and gene significance for M ϕ 1/M ϕ 2 (Fig. 3C). Then, we screened
250 the hub genes in the network based on the number of connections between nodes. CytoHubba was
251 used to calculate the top 40 hub genes (Fig. 4B). Intersections between the two sets of hub genes
252 were established. Intersections for the genes in blue, turquoise, and green modules were 15, 15, and
253 19, respectively (Fig. 4C). Finally, univariate analysis revealed that RPS9, DUT, and KIAA0430
254 genes were significantly associated with implantation failure in the blue, turquoise, and green
255 modules (Fig. 4D).

256 **3.4 Lab and external verification of hub genes expression and correlation with M ϕ 1/ M ϕ 2**

257 We first validated the altered mRNA expression levels of DUT, RPS9, and KIAA0430 in
258 endometrial tissues. Compared with the control group, the expression of all three genes ($P=0.029$,
259 0.028 , and 0.0006 for DUT, RPS9, and KIAA0430, respectively) in patients with IVF failure was
260 significantly downregulated (Fig.5 A).

261 Then, we selected M ϕ s datasets in GSE5099 to verify the association between the above screened
262 genes and macrophage polarization. As shown in Fig. 5B, RPS9, DUT, and KIAA0430 ($R=0.79$,
263 0.98 , 0.97) genes exhibited high relation with M ϕ 1 and M ϕ 2.

264 Then, we performed correlation analysis by macrophages count and qPCR results to verify the
265 association between the above screened genes and M ϕ 1/M ϕ 2. As shown in Fig. 5C, RPS9, DUT, and
266 KIAA0430 genes exhibited significant correlation with M ϕ 1/ M ϕ 2, as 0.52 ($P=0.058$), 0.50
267 ($P=0.048$), and 0.55 ($P=0.027$), respectively (Fig. 5C).

268 Subsequently, GSEA results for the three genes were consistent with our previous findings, that is
269 ribosomal (RPS9, DUT and KIAA0430), lysosome (DUT), and proteasomal (RPS9 and KIAA0430),
270 respectively (Fig. 5E).

271 **3.5 Establishment and validation of an artificial neural network prognostic model**

272 Then, we used a deep machine learning algorithm (ANN) to evaluate the predictive power of selected
273 hub genes for defective endometrial receptivity. First, we set the number of units in the hidden layer
274 of the GSE58144 dataset. The model achieved the highest prediction accuracy of 98.3% when the
275 hidden layer was set to 24 (Fig. 6A).

276 Further, we validated this prognostic model using the GSE165004 dataset. Aforementioned hub
277 genes were incorporated into the ANN prognostic model. Based on an earlier finding, we set the
278 number of units in the hidden layer to 24 and performed 100 cycles of simulation to improve the
279 prognostic accuracy (Fig. 6B). As a further verification that the ANN model is the optimal model for
280 implantation failure prediction, we also established a prediction model based on logistic regression.

281 In Fig. 6C, expression levels of the three hub genes were found to be significantly different between
282 the two groups, consistent with the results of the GSE58144 dataset. Also, the risk score, based on
283 the logistic regression, showed the ability for defective endometrial receptivity identification. The
284 Nomogram based on logistic regression is shown in Fig.6D. Prognostic results were averaged and
285 plotted as ROC, and were found to compare to those by modules and hub genes. As result, the AUC
286 of the ANN model was 0.975 (95% CI 0.945-1), significantly better than that of nomogram model,
287 DUT, RPS9, and KIAA0430 ($p=0.0439$, 9.27×10^{-6} , 1.15×10^{-6} , and 5.33×10^{-4}), as shown in Fig. 7A.
288 Sensitivity, specificity, YI, PPV, and NPV of the ANN model were 89.58 (95% CI 77.3 - 96.5),
289 95.83 (95% CI 78.9 - 99.9), 0.854, 97.7 (95% CI 86.3 - 99.7), and 82.1 (95% CI 66.6 - 91.4), superior
290 to those of the nomogram model and other hub genes, as shown in Fig. 7B.

291 4. Discussion

292 The altered immune microenvironment in the uterine cavity, an essential aspect of endometrial
293 receptivity, is a crucial factor for a successful IVF(24). However, immune-related factors have been
294 seriously underestimated when used to assess endometrial receptivity. In this study, we found that the
295 balance of the ratio between M ϕ 1 and M ϕ 2 is an important factor that affects endometrial receptivity
296 for patients. Then, we screened different biological functional gene modules and obtained hub genes
297 that may associate with M ϕ 1/M ϕ 2 and developed a machine deep learning prognostic model with an
298 excellent predictive performance through the artificial neural network approach.

299 Macrophages can be classified into the activated M ϕ 1 and the alternatively activated M ϕ 2 based on
300 phenotypes and function. The balance of macrophage ratios is important for WOI and embryonic
301 implantation in the endometrium(6). However, the type of macrophage dominating the mid-secretory
302 phase has not yet been established. Russell et al. (25) reported a significant increase in M ϕ 2 during
303 the luteal phase, which are thought to contribute to the establishment of maternal immune tolerance
304 to fetal antigens at the onset of implantation. Conversely, Diao et al. (24) reported that the abundance
305 of M ϕ 2 was significantly lower in control subjects than in patients with failed embryonic
306 implantation. Some studies have also suggested that, during implantation, activated M ϕ 1 produce
307 inflammatory cytokines and mediators, such as IL-6, IL-1 β , TNF- α , and nitric oxide, inducing a pro-
308 inflammatory response and promoting embryonic attachment to the decidua. Consistent with these
309 observations, in this study, immune infiltration analysis and immunofluorescence validation revealed
310 M ϕ 1/M ϕ 2 alterations in patients in the reduced endometrial receptivity group compared to the control
311 group. This finding confirms the importance of the balance of macrophage polarization for
312 embryonic implantation.

313 Factors that induce macrophage infiltration into the endometrium in mid-secretory phase, including
314 chemokines, colony-stimulating factor (CSF)-1, and granulocyte macrophage-colony-stimulating
315 factor (GM-CSF) are abundantly secreted by endometrial stromal cells in response to hormonal
316 stimulation. Vascular endothelial growth factor receptor-1 (VEGFR-1) performs an important role in
317 macrophage recruitment and angiogenesis at the implantation site. Macrophages have a high potential
318 for plasticity and can modify their functions depending on the changing microenvironment in tissues
319 and are, therefore, involved in different physiological functions and disease development. This study
320 identified three highly correlated modules (antigen processing and presentation of exogenous peptide
321 antigen via MHC class I, TAP-dependent, phagosome acidification, and interleukin-1-mediated
322 signaling pathway) in macrophage polarization in the endometrium that affect macrophage functions
323 and their effects on endometrial receptivity through different aspects. The main pathways of the
324 modules were ribosome, lysosome and proteasome pathways. Then, we selected representative genes
325 (DUT, RPS9 and KIAA0430) in each gene module. These genes and their closely related are
326 important in the homeostasis of macrophage polarization and maintenance of favourable endometrial
327 receptivity (Fig. 8).

328 In blue module, the principal biological functions performed by the gene cluster is antigen processing
329 and presentation of exogenous peptide antigen via MHC class I, TAP-dependent. MHC class I plays
330 an intermediate role in the regulation of macrophage phagocytosis. As part of local immunity,
331 macrophages recognize antigens in MHC class I and present them to T cells which recognize the
332 MHC-antigen complex through their T cell receptors, which requires additional costimulatory and
333 cytokine signals. Macrophages can thus mediate and provide the costimulatory signals and cytokine
334 secretion required for effective T-cell activation (26). M ϕ 1 secrete various cytokines, including tumor
335 necrosis factor alpha (TNF- α), interleukin (IL)-1 α , and IL-6, which may be closely associated with
336 endometrial decidualization and embryonic implantation process. M ϕ 2 maturation can be induced by

337 various cytokines, including IL-4, IL-13, glucocorticoids, as well as M-CSF/CSF1, and together with
338 Tregs, they promote tissue remodeling and regeneration, wound healing, and anti-inflammation in the
339 endometrial tissue. Altered expression levels of some cytokines, such as TNF- α and IL-1 β , can affect
340 the polarization shift between M ϕ 1 and M ϕ 2, impacting reproductive outcomes. Meanwhile, class I
341 expression may be critical for avoidance of immunological rejection(27). Its hub gene RPS9, a
342 component of the ribosomal 40s subunit, is an important factor in macrophage activation and
343 polarization through its protein translation function. Various cytokines, such as IFN- γ , IL-10a, and
344 IL-6 have been shown to regulate ribosomes through receptors, thereby affecting macrophage
345 metabolism as well as mRNA translation (28). Silvia et al. (29) evaluated endometrial receptivity-
346 related pathways and found that the ribosomal pathway is the most relevant for endometrial fertility.
347 Furthermore, the result of GSEA showed a negative correlation between RPS9 and proteasome.
348 According to Fan et al. (30), molecules such as ribosomes in macrophages can be hydrolyzed by the
349 proteasome through ubiquitination. In addition, inhibition of this pathway has also been shown to
350 have positive implications in protection of macrophages as well as the periphery from hypoxia-
351 reoxygenation injury. In this study, RPS9 was significantly differentially expressed in IF and control
352 groups for both GSE58144 and GSE165004 datasets. These findings imply that module of antigen
353 processing and presentation of exogenous peptide antigen via MHC class I in macrophage
354 polarization play important roles in endometrial receptivity.

355 As for the turquoise module, the genes are enriched in the biological process of phagosome
356 acidification, which is directly linked to the phagocytic function of macrophages. DUT, as the hub
357 gene, were enriched in lysosome and ribosome pathways by its related genes in the GSE5099 dataset,
358 consistent with its module. Phagocytosis and antigen presentation by macrophages is dependent on
359 phagosome and lysosomal activity. Phagosome-like compartments containing antigen at some stages
360 fused with lysosomes to form a phagolysosome. Correspondingly, according to Ariza et al. (31), the

361 regulation of DUT to macrophages depends on their phagocytosis. DUT (dUTPase) , an essential
362 enzyme during nucleotide metabolism, hydrolyzes dUTP to dUMP and pyrophosphate. Alternative
363 splicing of this gene leads to different isoforms that are localized in the mitochondria or nucleus.
364 dUTPase modulates innate immunity in human primary monocyte-derived macrophages through toll-
365 like receptor (TLR) 2 leading to NF- κ B activation and the production of pro-inflammatory cytokines.
366 This process is achieved via macrophage phagocytosis of exosomes containing dUTPase. Then,
367 interferon (IFN)- γ , lipopolysaccharide (LPS), or granulocyte macrophage-colony-stimulating factor
368 induce macrophage maturation towards the M ϕ 1, which activates Toll-like receptor signaling
369 pathways, thereby playing a crucial role in clearance of residual fibers and tissue debris, and in the
370 synthesis of pro-inflammatory cytokines and growth factors. In addition, Wang et al(31). reported
371 that DUT activation led to the production of large amounts of mtDNA, which bound the
372 mitochondrial ribosomal proteins to co-synthesize mitochondria-associated proteins, further
373 demonstrating the association between DUT and the ribosomal pathway. Therefore, enrichment
374 analysis of the turquoise gene module in endometrial tissues and the DUT in macrophage GSE5099
375 dataset revealed a close association among DUT, phagosome acidification, and the aforementioned
376 two pathways, which affect the M ϕ 1/M ϕ 2 ratio in patients who were in the mid-secretory phase.

377 The green module's biological function was enriched in the interleukin-1-mediated signaling
378 pathway, which is vital for macrophage functions and polarization. Elevated expression levels of
379 cytokines such as TNF- α in the early stages promote macrophages polarization, as well as the
380 synthesis and secretion of IL-1 by macrophages. In addition, IL-1 in the early stages can act on
381 interleukin-1-mediated signaling pathway to promote other cytokines' synthesis and secretion, is
382 intimately involved in the regulation of the ribosome pathway (32). Its hub gene, KIAA0430, also
383 known as meiosis regulator and mRNA stability factor 1 (MARF1), encodes a putative peroxisomal
384 protein, which can silence targeted mRNA and inhibit gene expression (33). It can regulate the

385 translational function of ribosomes in the manner above, consistent with the result that it was
386 enriched in the ribosome pathway in the GSE5099 dataset. Meanwhile, we found that gene
387 enrichment in the green module, where KIAA0430 is located, was closely related to negative
388 regulation of the proteasome pathway. The negative correlation between KIAA0430 and the
389 proteasome pathway was verified in the macrophage GSE5099 dataset. Proteasomes are protein
390 disruption devices that are involved in many essential cellular functions, such as cell cycle regulation,
391 cell differentiation, signal transduction pathways, antigen processing for proper immune responses,
392 stress signaling, inflammatory responses, and apoptosis. Moreover, they are involved in macrophage
393 polarization. Cytokines such as IFN- γ and TNF- α have been shown to regulate macrophage functions
394 by moderating the proteasome pathway. Han et al. (34) reported that proteasomes in endometrial
395 stromal cells can mediate diminished protein stabilities of HOXA10, a histone important for
396 promoting endometrial decidualization, leading to a defective endometrial receptivity. In contrast,
397 negative regulation of the proteasome pathway by KIAA0430 facilitates the maintenance of
398 favourable endometrial receptivity.

399 Although macrophage polarization is of great importance in pregnancy, few are available to diagnose
400 reproductive prognosis, mainly because of subjectivity of cell counts by immunohistochemistry and
401 difficulty with standardization. Moreover, immune cell infiltration dynamics leads to the possibility
402 of some systematic errors. Therefore, in this study, we used macrophage polarization-related factors
403 as predictors for reproductive prognostic outcomes. To ensure that genes included in the prognostic
404 model are representative of certain molecular functions or structures, we performed gene selection
405 through the WGCNA approach. Then, we used ANN and logistic regression approaches to establish a
406 prognostic model. Traditional models were often constructed through the regression approach. Model
407 optimization requires the inclusion of factors that are both normally distributed and independent. For
408 factors with small values, the weight of their impact on the outcome is often ignored because of their

409 low coefficients. The ANN model, however, can weigh each feature variable according to its
410 importance and then perform the summation of activity function, thus, it requires fewer factors to
411 provide a more accurate classification. Also, it was certainly demonstrated in our study that the ANN
412 was superior to the traditional logistic regression-based Nomogram in terms of IVF failure
413 prediction. Although we found an imbalance between M ϕ 1 and M ϕ 2, we performed the diagnosis by
414 expression of factors in different gene modules instead of direct microscopic counts to improve
415 reproducibility of the results and reduce measurement errors associated with subjectivity. The
416 predictive accuracy of the model was up to 98.3% in the GSE58144 dataset, while its AUC was
417 0.975 in the validation GSE165004 dataset, significantly better than the predictive method with a
418 single factor and regression approach. Its performance was also superior to the conventional
419 endometrial receptivity examinations, such as ultrasound for endometrial thickness (>7 mm) with a
420 sensitivity of 99% and a specificity of 3% (2). The significance of this predictive method is that it
421 effectively determines the receptive status of the endometrium. Jena et al. (6) reported that there is a
422 dynamic balance of macrophage polarization patterns in the endometrium in response to the
423 menstrual cycle, suggesting that this model is appropriate for assessing endometrial receptivity in
424 patients with IVF failure due to WOI changes. Importantly, uterine cavity procedures (induced
425 abortion, adhesiolysis, or polypectomy), inflammatory responses and transient immune dysregulation
426 (dysbacteriosis or endometritis) due to stress can lead to embryonic implantation failure (35, 36).
427 However, this model is highly correlated with the immune environment and is appropriate for
428 informing optimal timing of natural or IVF pregnancies in such patients. For patients, assessment of
429 endometrial receptivity using this tool is beneficial in identifying the cause and predicting the
430 immediate outcome of IVF.

431 This study has its advantages. Firstly, the effects of 22 immune cell infiltrations on embryo
432 implantation were explored for the first time, screening factors of significance. Secondly, instead of

433 applying the commonly used PCA and other dimensionality reduction methods, we performed a hub
434 gene selection in the module by WGCNA, which ensured the representativeness of the characteristics
435 data and reduced the number of items to be examined. This dramatically saves tests cost in clinical
436 application. Finally, a non-regression model was used to establish predicted reproductive outcomes,
437 reducing the influence of data characteristics and weights on prediction. This experiment preliminary
438 validated changes in the ratio between M ϕ 1 and M ϕ 2 and established a prognostic model, however,
439 there are some limitations. First, other cheaper assays, such as qRT-PCR or ELISA, were not
440 performed for the test of the model, which needs to be validated through further large sample
441 experiments. Second, for the mechanistic study, only enrichment analysis was performed, which are
442 all based on mRNA expression levels. Therefore, it was not possible to observe the effects of changes
443 in translational or post-translational protein levels for mechanism prediction, which should be
444 validated further. Importantly, Lab experiments results and cross-validation between multiple data
445 sets guarantee reliability of the mechanism as well as the ANN model. In short, based on our results,
446 the consistency of validation, as analysed by different methods and datasets, was mutually confirmed.

447 In summary, the balance between M ϕ 1 and M ϕ 2 is essential for the pregnancy process. Gene
448 modules associated with biological processes of antigen processing and presentation of exogenous
449 peptide antigen via MHC class I, TAP-dependent, phagosome acidification, and interleukin-1-
450 mediated signaling pathway can impact macrophage polarization that ameliorate endometrial
451 receptivity. Furthermore, the established ANN model based on hub genes can effectively assess
452 endometrial receptivity to inform patients' reproductive outcomes and individualized clinical
453 management strategies.

454 5. List of abbreviations

WOI	window of implantation
-----	------------------------

(R)IF	(repeated) implantation failure
NK	Natural killer
WGCNA	weighted gene co-expression network analysis
ANN	artificial neural network
DER	decreased endometrial receptivity
RMA	Robust multi-array average
BSA	bovine serum albumin
PBS	phosphate-buffered saline
GO	Gene Ontology
BP	Biological Process
CC	Cellular Component
MF	Molecular Function
KEGG	Kyoto Encyclopedia of Genes and Genome
GSEA	Gene-set enrichment analysis
qRT-PCR	Quantitative Real-Time PCR Analysis
ROC	receiver operating characteristic
PPV	positive predictive value
NPV	negative predictive value
MS	module significance
CSF-1	colony-stimulating factor

GM-CSF	granulocyte macrophage-colony-stimulating factor
VEGFR-1	Vascular endothelial growth factor receptor-1
IFN- γ	Interferon
LPS	lipopolysaccharide
TNF- α	tumor necrosis factor alpha
IL-1 α	interleukin.

455

456 **6. References**

- 457 1. Lessey BA, Young SL. What exactly is endometrial receptivity? *Fertility and sterility*.
458 2019;111(4):611-7.
- 459 2. Craciunas L, Gallos I, Chu J, Bourne T, Quenby S, Brosens JJ, et al. Conventional and modern
460 markers of endometrial receptivity: a systematic review and meta-analysis. *Hum Reprod Update*.
461 2019;25(2):202-23.
- 462 3. Ruiz-Alonso M, Blesa D, Díaz-Gimeno P, Gómez E, Fernández-Sánchez M, Carranza F, et al.
463 The endometrial receptivity array for diagnosis and personalized embryo transfer as a treatment
464 for patients with repeated implantation failure. *Fertility and sterility*. 2013;100(3):818-24.
- 465 4. Ben Rafael Z. Endometrial Receptivity Analysis (ERA) test: an unproven technology. *Hum*
466 *Reprod Open*. 2021;2021(2):hoab010.
- 467 5. Zhang Y-H, He M, Wang Y, Liao A-H. Modulators of the Balance between M1 and M2
468 Macrophages during Pregnancy. *Front Immunol*. 2017;8:120.
- 469 6. Jena MK, Nayak N, Chen K, Nayak NR. Role of Macrophages in Pregnancy and Related
470 Complications. *Archivum immunologiae et therapeuticae experimentalis*. 2019;67(5):295-309.
- 471 7. Li Z-H, Wang L-L, Liu H, Muyayalo KP, Huang X-B, Mor G, et al. Galectin-9 Alleviates LPS-
472 Induced Preeclampsia-Like Impairment in Rats via Switching Decidual Macrophage Polarization
473 to M2 Subtype. *Front Immunol*. 2018;9:3142.

- 474 8. Schork NJ. Genetics of complex disease: approaches, problems, and solutions. *Am J Respir Crit*
475 *Care Med.* 1997;156(4 Pt 2):S103-S9.
- 476 9. Lan H, Chen M, Flowers JB, Yandell BS, Stapleton DS, Mata CM, et al. Combined expression
477 trait correlations and expression quantitative trait locus mapping. *PLoS Genet.* 2006;2(1):e6.
- 478 10. Li B, Wang S, Duan H, Wang Y, Guo Z. Discovery of gene module acting on ubiquitin-mediated
479 proteolysis pathway by co-expression network analysis for endometriosis. *Reprod Biomed Online.*
480 2021;42(2):429-41.
- 481 11. Hou Q, Bing ZT, Hu C, Li MY, Yang KH, Mo Z, et al. RankProd Combined with Genetic
482 Algorithm Optimized Artificial Neural Network Establishes a Diagnostic and Prognostic
483 Prediction Model that Revealed C1QTNF3 as a Biomarker for Prostate Cancer. *EBioMedicine.*
484 2018;32:234-44.
- 485 12. Zhang Z. A gentle introduction to artificial neural networks. *Ann Transl Med.* 2016;4(19):370.
- 486 13. Gautier L, Cope L, Bolstad BM, Irizarry RA. *affy*--analysis of Affymetrix GeneChip data at the
487 probe level. *Bioinformatics.* 2004;20(3):307-15.
- 488 14. Li Y, Bai W, Zhang L. The Overexpression of CD80 and ISG15 Are Associated with the
489 Progression and Metastasis of Breast Cancer by a Meta-Analysis Integrating Three Microarray
490 Datasets. *Pathol Oncol Res.* 2020;26(1):443-52.
- 491 15. Yoneya T, Miyazawa T. Integration of pre-normalized microarray data using quantile correction.
492 *Bioinformatics.* 2011;5(9):382-5.
- 493 16. Shakya K, Ruskin HJ, Kerr G, Crane M, Becker J. Comparison of microarray preprocessing
494 methods. *Adv Exp Med Biol.* 2010;680:139-47.
- 495 17. Forero DA, Guio-Vega GP, González-Giraldo Y. A comprehensive regional analysis of genome-
496 wide expression profiles for major depressive disorder. *J Affect Disord.* 2017;218:86-92.
- 497 18. Li B, Duan H, Wang S, Li Y. Ferroptosis resistance mechanisms in endometriosis for diagnostic
498 model establishment. *Reprod Biomed Online.* 2021.
- 499 19. Database resources of the National Center for Biotechnology Information. *Nucleic Acids Res.*
500 *NCBI Resource Coordinators,* 2015;43(Database issue):D6-17.
- 501 20. Newman AM, Steen CB, Liu CL, Gentles AJ, Chaudhuri AA, Scherer F, et al. Determining cell
502 type abundance and expression from bulk tissues with digital cytometry. *Nat Biotechnol.*

- 503 2019;37(7):773-82.
- 504 21. Ghazalpour A, Doss S, Zhang B, Wang S, Plaisier C, Castellanos R, et al. Integrating genetic and
505 network analysis to characterize genes related to mouse weight. *PLoS Genet.* 2006;2(8):e130.
- 506 22. Langfelder P, Horvath S. WGCNA: an R package for weighted correlation network analysis. *BMC*
507 *Bioinformatics.* 2008;9:559.
- 508 23. Wang S, Li B, Duan H, Wang Y, Shen X, Dong Q. Abnormal expression of connective tissue
509 growth factor and its correlation with fibrogenesis in adenomyosis. *Reprod Biomed Online.*
510 2021;42(3):651-60.
- 511 24. Diao L, Cai S, Huang C, Li L, Yu S, Wang L, et al. New endometrial immune cell-based score
512 (EI-score) for the prediction of implantation success for patients undergoing IVF/ICSI. *Placenta.*
513 2020;99:180-8.
- 514 25. Russell P, Anderson L, Lieberman D, Tremellen K, Yilmaz H, Cheerala B, et al. The distribution
515 of immune cells and macrophages in the endometrium of women with recurrent reproductive
516 failure I: Techniques. *Journal of reproductive immunology.* 2011;91(1-2):90-102.
- 517 26. Guerriero JL. Macrophages: Their Untold Story in T Cell Activation and Function. *Int Rev Cell*
518 *Mol Biol.* 2019;342:73-93.
- 519 27. Davies CJ, Fisher PJ, Schlafer DH. Temporal and regional regulation of major histocompatibility
520 complex class I expression at the bovine uterine/placental interface. *Placenta.* 2000;21(2-3):194-
521 202.
- 522 28. Su X, Yu Y, Zhong Y, Giannopoulou EG, Hu X, Liu H, et al. Interferon- γ regulates cellular
523 metabolism and mRNA translation to potentiate macrophage activation. *Nat Immunol.*
524 2015;16(8):838-49.
- 525 29. Pérez-Debén S, Bellver J, Alamá P, Salsano S, Quiñonero A, Sebastian-Leon P, et al. iTRAQ
526 comparison of proteomic profiles of endometrial receptivity. *J Proteomics.* 2019;203:103381.
- 527 30. Fan T, Huang Z, Wang W, Zhang B, Xu Y, Mao Z, et al. Proteasome inhibition promotes autophagy
528 and protects from endoplasmic reticulum stress in rat alveolar macrophages exposed to hypoxia-
529 reoxygenation injury. *J Cell Physiol.* 2018;233(10):6748-58.
- 530 31. Wang Y-P, Sharda A, Xu S-N, van Gastel N, Man CH, Choi U, et al. Malic enzyme 2 connects the
531 Krebs cycle intermediate fumarate to mitochondrial biogenesis. *Cell Metab.* 2021;33(5).

- 532 32. Li B, Duan H, Wang S, Wang Y, Chang Y, Guo Z, et al. Hierarchical cluster analysis in the study
533 of the effect of cytokine expression patterns on endometrial repair and receptivity after
534 hysteroscopic adhesiolysis. *Ann Transl Med.* 2021;9(9):746.
- 535 33. Nishimura T, Fakim H, Brandmann T, Youn J-Y, Gingras A-C, Jinek M, et al. Human MARF1 is
536 an endoribonuclease that interacts with the DCP1:2 decapping complex and degrades target
537 mRNAs. *Nucleic Acids Res.* 2018;46(22):12008-21.
- 538 34. Han K, Zhou Q. Skp2 Deteriorates the Uterine Receptivity by Interacting with HOXA10 and
539 Promoting its Degradation. *Reprod Sci.* 2021;28(4):1069-78.
- 540 35. Ke L, Lin W, Liu Y, Ou W, Lin Z. Association of induced abortion with preterm birth risk in first-
541 time mothers. *Sci Rep.* 2018;8(1):5353-.
- 542 36. Zhao X, Zhao Q, Zhu X, Huang H, Wan X, Guo R, et al. Study on the correlation among
543 dysbacteriosis, imbalance of cytokine and the formation of intrauterine adhesion. *Ann Transl Med.*
544 2020;8(4):52.

545

546 **7. Declarations**

547 **Competing interests**

548 The authors declare that the research was conducted in the absence of any commercial or financial
549 relationships that could be construed as a potential conflict of interest.

550 **Author Contributions**

551 **BL**, Conception and design, Collection and assembly of data, Manuscript writing, Final approval of
552 manuscript, Administrative support; **HD**, Conception and design, Manuscript writing, Administrative
553 support, Final approval of manuscript; **SW**, Provision of study materials or patients, Manuscript
554 writing, Final approval of manuscript; **JW** and **YL** Manuscript writing, Final approval of manuscript.

555 **Funding**

556 This study was financially supported by the National Key Research and Development Program of
557 China (2018YFC1004803).

558 **Data Availability Statement**

559 The raw data supporting the conclusions of this article will be made available by the authors, without
560 undue reservation.

561 **Ethics approval and consent to participate**

562 Ethical approval for this study was obtained from the Research Ethics Committee of the Beijing
563 Obstetrics and Gynecology Hospital. Experiments were performed (under protocol number 2017-
564 KY-082-02) based on the Helsinki Declaration of 1975 (revised in 2013).

565 **Acknowledgments**

566 This study was financially supported by the National Key Research and Development Program of
567 China (2018YFC1004803). The paper is edited by Home for researchers editorial team. We also
568 thank the researchers of datasets GSE58144, GSE5099 and GSE165004 for their selfless sharing.

569 **Consent for publication**

570 All presentations have consent for publication.

571

572

573

Figures

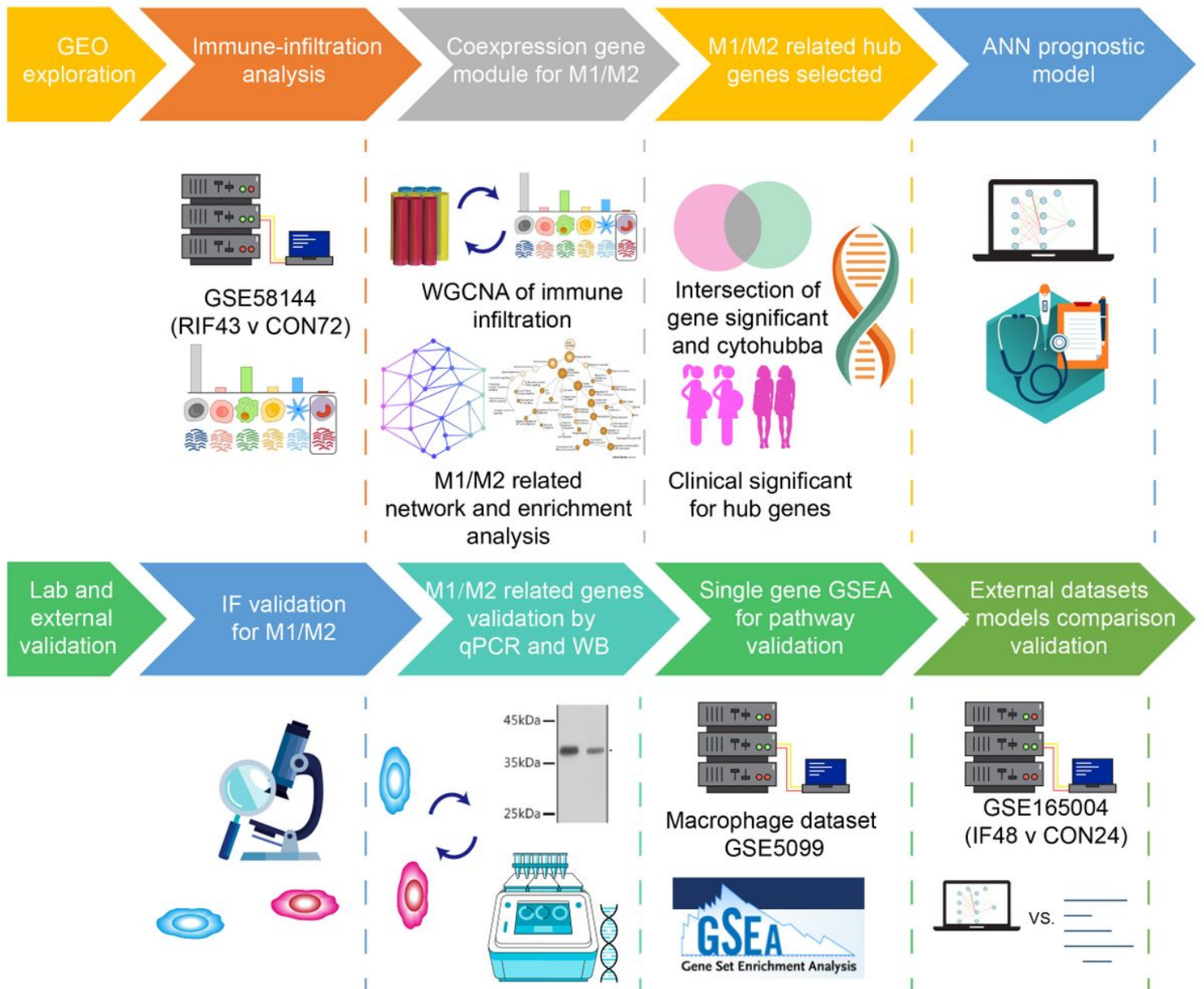


Figure 1

Schematic presentation of the study design. (R)IF= (recurrent) implantation failure, IF= Immunofluorescence, WB= Western blot, ANN= artificial neural network and GSEA= Gene-set enrichment analysis.

Figure 2

Immune infiltration analysis and M Φ 1 to M Φ 2 ratio. A) Bar plots for 22 immune cells in endometrial mixed tissue samples. B) Violin plots for immune cells in the IF (n=16) and control (n=14) groups. Blue color represents the IF group while the Red color represents the control group. C) Comparisons of

MΦ1/MΦ2 between the IF and control groups from the GSE58144 dataset. D) Immunofluorescence detection of MΦ1 and MΦ2. CD86 (green) and CD68 (red) positivity represent MΦ1. CD163 (green) and CD68 (red) positivity represent MΦ2. White arrows in the overlay represent positive cells. E) Immunofluorescence validation of MΦ1/MΦ2 comparisons in the IF and control groups. IF= Implantation failure.

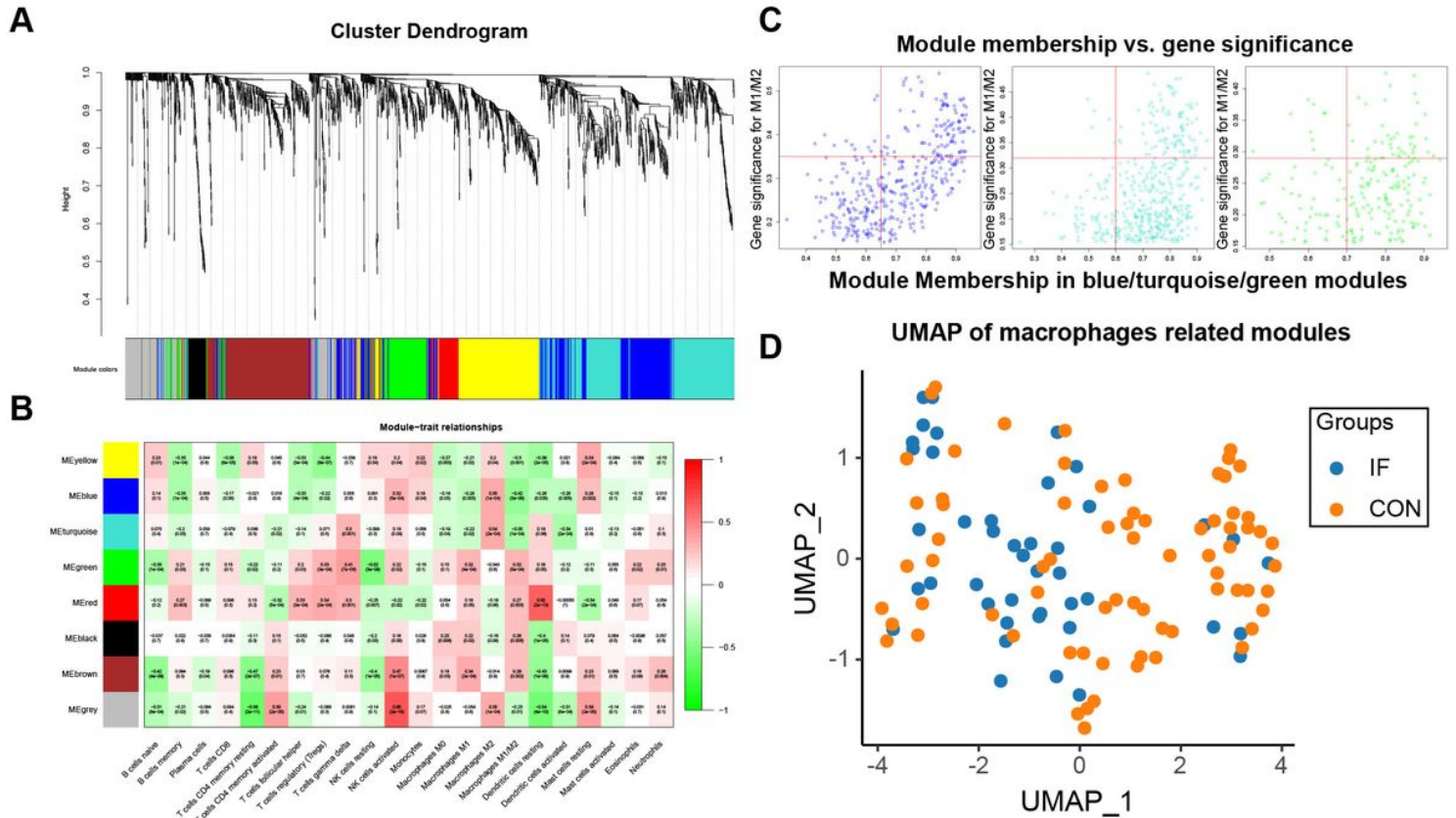


Figure 3

MΦ1/MΦ2 related WGCNA and module enrichment analyses. A) Visual representations of the gene co-expression network. Hierarchical clustering of 2,185 genes and visualization of gene module partitioning. Coloured bars (below) directly correspond to module (colour) designation for gene clusters. One can visualize where in the clustering dendrogram the gene modules are defined. B) Heatmap showing the average genetic significance of each particular module across immune infiltration levels. C) The correlation between module membership and gene significance in the three modules. D) Simple characterization were analyzed using UMAP by genes in selected three macrophages related modules.

Figure 4

Module enrichment analyses and hub gene selection. A) Enrichment analysis. The left side is the gene (the shade of the colour represents the gene's fold change), while the right side are the different GO/KEGG terms. Connected bands indicate that a gene is in its corresponding GO/KEGG terms. B) Co-expression

network diagram. Top 40 hub genes were selected and visualized. Color shades represent the number of connections. C) Venn plot for gene screening. D) Univariate analysis of screened genes.

Figure 5

Validation of hub genes expression and correlations with M Φ 1/ M Φ 2. A) Validation of mRNA expression of hub genes in IF (n=8) and control (n=8). B) correlation between hub genes and M Φ 1/M Φ 2. C) Verification of correlation between hub genes and M Φ 1/M Φ 2. D) Pathway validation of hub genes by GSEA.

Figure 6

Prognostic models' establishment and vilification. A) Schematic presentation of the ANN model for predicting implantation failure. Dark green represent transmission of information from hub genes. Green and red colours represent positive and negative weights, respectively. Light blue represents the bias applied to hidden neurons. B) Average accuracy of each number of units. Twenty four units had the greatest accuracy (98.3%). C) Validation for predictive values of DUT, RPS9, KIAA0430, and the risk model based on logistic regression. D) Nomogram diagnostic model based on logistic regression.

Figure 7

Assessment for the models and genes in implantation prediction. A) ROC curve for ANN, Nomogram, DUT, RPS9 and KIAA0430 (left), and AUC comparison between models and genes. B) Diagnostic efficacies for the models and genes. YI=Youden index, PPV=positive predictive value, and NPV=negative predictive value.

Figure 8

Regulation of mid-secretory macrophage mechanisms. Macrophage polarization can ameliorate endometrial receptivity through regulation of hub genes, DUT, RPS9, and KIAA0430, mediating ribosomal as well as proteasomal pathways for endometrial decidualization.

Supplementary Files

This is a list of supplementary files associated with this preprint. Click to download.

- [SupplementaryTable.docx](#)